



HAL
open science

Coherent beam combining of high power quasi continuous wave tapered amplifiers

P. Albrodt, M. Niemeyer, P. Crump, J. Hamperl, F. Moron, Patrick Georges, Gaëlle Lucas-Leclin

► **To cite this version:**

P. Albrodt, M. Niemeyer, P. Crump, J. Hamperl, F. Moron, et al.. Coherent beam combining of high power quasi continuous wave tapered amplifiers. *Optics Express*, 2019, 27 (20), pp.27891-10.1364/OE.27.027891 . hal-02332526

HAL Id: hal-02332526

<https://hal.science/hal-02332526>

Submitted on 24 Oct 2019

HAL is a multi-disciplinary open access archive for the deposit and dissemination of scientific research documents, whether they are published or not. The documents may come from teaching and research institutions in France or abroad, or from public or private research centers.

L'archive ouverte pluridisciplinaire **HAL**, est destinée au dépôt et à la diffusion de documents scientifiques de niveau recherche, publiés ou non, émanant des établissements d'enseignement et de recherche français ou étrangers, des laboratoires publics ou privés.

Coherent beam combining of high power quasi continuous wave tapered amplifiers

P. ALBRODT,¹ M. NIEMEYER,² P. CRUMP,² J. HAMPERL,¹ F. MORON,¹ P. GEORGES,¹ AND G. LUCAS-LECLIN,^{1,*}

¹Laboratoire Charles Fabry, Institut d'Optique Graduate School, CNRS, Université Paris-Saclay, 2 Avenue Augustin-Fresnel, 91127 Palaiseau, France

²Ferdinand-Braun-Institut, Leibniz-Institut für Höchstfrequenztechnik, Gustav-Kirchhoff-Str. 4, 12489 Berlin, Germany

*gaelle.lucas-leclin@institutoptique.fr

Abstract: We demonstrate coherent beam combining of four high brightness tapered amplifiers in pulsed, quasi continuous wave (QCW) operation, seeded by a 976 nm laser diode. The maximum power of 22.7 W was achieved with > 64 % combining efficiency in a close to diffraction limited beam. We discuss turn-on dynamics of tapered amplifiers operated in pulsed mode in detail.

© 2019 Optical Society of America under the terms of the OSA Open Access Publishing Agreement

1. Introduction

The power and brightness of laser diodes are continuously increasing and as the cost per watt is decreasing at the same time, they become more attractive for industrial application requiring high brightness [1]. It is however necessary to make use of beam combining technologies in order to meet the power requirements in this regard [2]. Especially spectral beam combining is a widely used approach for development of high brightness diode laser systems [3,4], the ultimate limitation is however the power available within a certain spectral linewidth. Coherent beam combining (CBC) relies on constructive interference of several separate beams and allows to scale the power available within a very narrow spectral bandwidth in a beam with nearly diffraction limited beam quality. CBC with diode lasers has been demonstrated in many different external cavity configurations [5–9] and in master oscillator power amplifier (MOPA) configurations [10,11]. The highest combined power has been achieved in a MOPA setup using large arrays of single mode amplifiers [11]. Using a few high brightness tapered amplifiers is a promising approach to reduce the complexity of CBC setups and yields in a higher power per element [12,13]. Operating those amplifiers in pulsed, quasi continuous wave (QCW) mode, allows even higher powers per amplifier to be reached as the devices are no longer limited by thermal rollover. However CBC of diode lasers has commonly been demonstrated in continuous wave (CW) operation and there are only few demonstrations of CBC of pulsed diode lasers [14]. Pulsed (QCW) semiconductor amplifiers are not in steady state but exhibit dynamic temperature changes. This consequently leads to a dynamic change of the accumulated phase and of the beam propagation parameters, which makes CBC with pulsed amplifiers more challenging. Additionally, high brightness pulsed sources with high spectral purity are in demand as NIR pump sources of solid state lasers and for nonlinear frequency conversion to address medical applications of modulated high power visible laser sources [15–17]. Furthermore CBC of pulsed tapered amplifiers may improve the performance of diode-laser-based portable differential absorption lidar systems used for atmospheric measurements [18,19].

We use a master oscillator power amplifier (MOPA) configuration with four parallel tapered amplifiers operated in QCW mode. Their coherent superposition is achieved in a filled aperture approach using standard beamsplitters as the combiner elements. The experimental setup is described in section 2. The performance of the tapered amplifiers is

characterized in section 3 especially regarding the dynamic change in phase as the devices are turned on. We observe and analyze effects associated with the operation of the pulsed amplifiers at high bias, which induce strong peak power fluctuations and deteriorate the seed line stability. Finally we demonstrate CBC of four high brightness tapered amplifiers in QCW mode and compare the results to operation in CW mode (see section 4).

2. Experimental setup

We used 5 mm long amplifiers consisting of a 1 mm long 4 μm wide ridge waveguide (RW) followed by a 4 mm long tapered section (TP, 6° taper angle). The facets of the devices were passivated and anti-reflection coated ($R_1 = 0.01\%$ for RW facet and $R_2 = 0.05\%$ for TP facet) [20] The epitaxial design of the devices was the so called ELOD2 design [21], having an extremely low vertical divergence, that has proven to maintain good beam quality at high drive currents in tapered laser format [21], with good results also in related designs in truncated tapered amplifier format [22]. We used individually mounted emitters instead of an array of amplifiers to achieve a simple modular setup and benefit from the efficient heat removal in each heatsink. The devices were mounted p-side up on CuW heat sinks onto C-mounts with separate electrical contacts for the currents I_{rw} into the RW and I_{tp} into the tapered section of each device respectively. An additional CuW heat spreader was also attached to the p-side of the tapered amplifier section for improved cooling. The C-mounts were fixed on individual temperature-stabilized mechanical mounts. The current into the RW was not pulsed as it has low impact on the total heat load of the device ($< 1\text{ W}$). We used small variations ($\pm 50\text{ mA}$) of the continuous current into the ridge section of each amplifier for phase-control [23]. We used Arroyo 4320-QCW laser diode drivers for the current into the tapered section of each device.

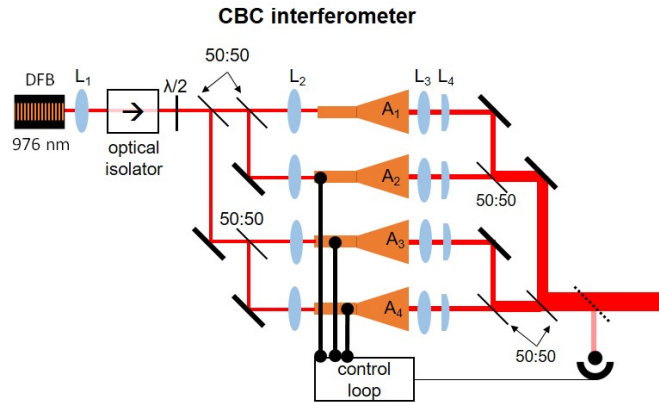


Fig. 1. Experimental setup of the CBC-interferometer with four high brightness tapered amplifiers (A_{1-4}). The currents into the DFB seed laser and the RWs of the amplifiers were continuous and only the currents into the taper of each amplifier were pulsed. (L_1 and L_2 aspheric lens $f = 8\text{ mm}$ $\text{NA} = 0.5$, L_3 aspheric lens $f = 2.35\text{ mm}$ $\text{NA} = 0.55$, L_4 cylindrical lens $f = 19\text{ mm}$).

The pulse durations were in the order of a few milliseconds (typically $\Delta t_{\text{QCW}} = 2\text{ ms}$) and a duty cycle of 10 %. The amplifiers were arranged in a multiarm-interferometer as shown in Fig. 1 similar to the experimental setup used in previous work [13]. The seed source was a 100 mW CW narrow linewidth ($< 20\text{ MHz}$) DFB laser at 976 nm. After optical isolation the beam was split using non-polarizing 50:50 beamsplitters. The seed power incident for each amplifier was 20 mW. The amplified beams were collimated in slow axis (SA) and fast axis (FA) individually and the astigmatism was corrected depending on the current into the tapered section. We used also 50:50 plate beamsplitters for recombining the beams in a filled

aperture approach. The intensity of a small part of the output beam (less than 0.5 %) was measured with a photodiode, delivering the signal for the microcontroller based closed-loop phase correction.

3. Investigation of the dynamics of the amplifiers

3.1 Optical power and beam quality

The QCW operation of the amplifiers with pulse lengths in the ms-range and duty cycles typically below 10 % allows testing the devices beyond the limitations normally set by CW thermal rollover. The influence of the reduced heat load in QCW on the optical output power is clearly visible in the measurements plotted in Fig. 2(a). While there is an onset of the thermal rollover for all four amplifiers at about 10 A in CW mode (dashed lines), this is not the case for QCW operation (solid lines) and the slope efficiency remains constant at about 0.7 W/A resulting in an output power > 9 W for all four amplifiers at 16 A. The output power for moderate currents < 8 A is identical in CW and QCW operation. The beam shapes at the imaged beam waist are shown for one typical amplifier (A3) in Fig. 2(b) for different currents into the tapered section in CW and QCW mode. The beam shapes shown in Fig. 2(b) in QCW mode were measured 0.8 ms after the start of the pulse with 50 μ s integration time. At this time, the device temperature and beam shape is stabilized. The observed shapes are typical for tapered amplifiers, with a close to diffraction limited central lobe containing most of the energy and lower intensity higher angle side lobes in the slow axis (SA). The intensity of the side lobes gradually increases at higher currents into the taper leading to decreased power content in the central lobe, which is given in percent for each bias point in Fig 2(b). The differences in the beam shapes between CW and QCW operation are minor at moderate currents but one can observe a significant degradation of the beam quality when the amplifiers are overdriven in QCW operation leading to a central lobe power content of 73 % at 16 A. The beam shapes of the four amplifiers were quite similar with minor differences in the central lobe power content at equal bias conditions (+/- 5 %), considering that the beam quality also depends on alignment tolerances for the coupling into the narrow RW.

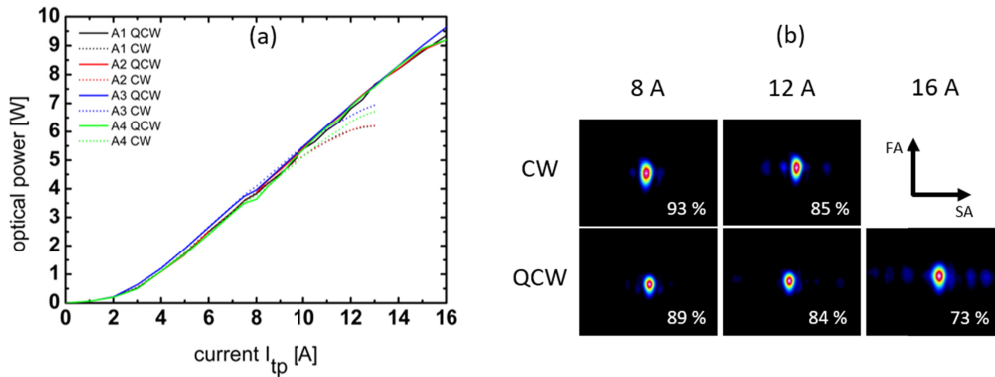


Fig. 2. (a) Optical output power versus drive current into the tapered section for the four amplifiers in CW and QCW operation. (b) Measurements of the beam shape at waist at different bias conditions. The power content in the central lobe was calculated with a 2D Gaussian fit of the central lobe. The integration time of the CCD camera was 50 μ s. (Bias conditions for all measurements: $P_m = 20$ mW, $I_{rw} = 350$ mA, $T = 25^\circ\text{C}$, $\Delta t_{qcw} = 1$ ms, 10 % duty cycle). See **Visualization 1** for the spatial turn-on dynamics in QCW mode. The video shows 20 images of the beam shape measured with 50 μ s integration time from the start to the end of the pulse.

Tapered lasers and amplifiers have a temperature induced wandering astigmatism that depends on the current into the tapered section [24,25]. This leads to a dynamic change in the beam shape in SA at the start of each QCW pulse. This effect is shown in the supplementary Visualization 1. We sampled 20 images of the beam shape into a short video showing that the

beam is focusing rapidly at the beginning of the pulse and then converges to a stable shape after about 500 μs . The measured 2nd moment beam diameter decreases from 1100 μm to 875 μm , which corresponds to a displacement of the waist in SA by about 80 % of the corresponding Rayleigh length at a current of 13 A into the tapered section. The spatial dynamics were similar for all four amplifiers in our setup. In order to ensure a good spatial overlap of the beams during the full pulse duration, it is therefore necessary to operate the different amplifiers at similar bias conditions in order to optimize the coherent beam combining efficiency.

3.2 Temperature - driven piston phase drift of pulsed amplifiers

The rise in temperature as the device is turned on does also increase the effective optical path length in the amplifier and leads to a drift of the accumulated phase in each amplifier. The piston phase drift is approximately proportional to the change in temperature. We measured the phase drift during the QCW pulses by overlapping the output beam from an amplifier with a reference beam as described in detail in [26]. Figure 3(a) shows the measurements for one amplifier at different currents into the tapered section. The amplitude of the piston phase drift increases with the current, and the experimentally measured phase drift was reproduced accurately at all bias points using the following fit function (Eq. 1), as seen in Fig. 3(a):

$$\varphi(t) = \varphi_0 + C \times t - \Delta\varphi_1 \times \exp\left[\frac{-t}{\tau_1}\right] - \Delta\varphi_2 \times \exp\left[\frac{-t}{\tau_2}\right]. \quad (1)$$

The time constants $\tau_{1,2}$ of the two exponential functions were found by fitting to be 0.1 ms and 1 ms respectively and these were independent of the current into the tapered section I_{tp} . The amplitudes of the exponential contributions $\Delta\varphi_{1,2}$ are proportional to I_{tp} and roughly equal for the two exponential contributions. The linear term $C \times t$ describes a linear increase in the average temperature of the heatsink during the pulse and is also proportional to I_{tp} . The amplitude of the overall change in piston is large, reaching 30π at 13 A for 5 ms long pulses. The dynamic variation in phase is however highly reproducible, consistent between samples and we propose it to be defined by the geometry and efficiency of the amplifiers, the heatsink and the rise-time of the current driver. We thus achieved a very good overlap of the piston phase drifts in all four amplifiers of the interferometer as shown in Fig. 3(b). We used small adjustments (± 0.5 A) of the pulsed current into the taper sections in order to achieve a piston phase drift of the same magnitude for all four amplifiers. The inset in Fig. 3(b) shows a zoom into the same data, where one can see that the relative differences in phase between the four amplifiers are in the range of $\pi / 10$ only.

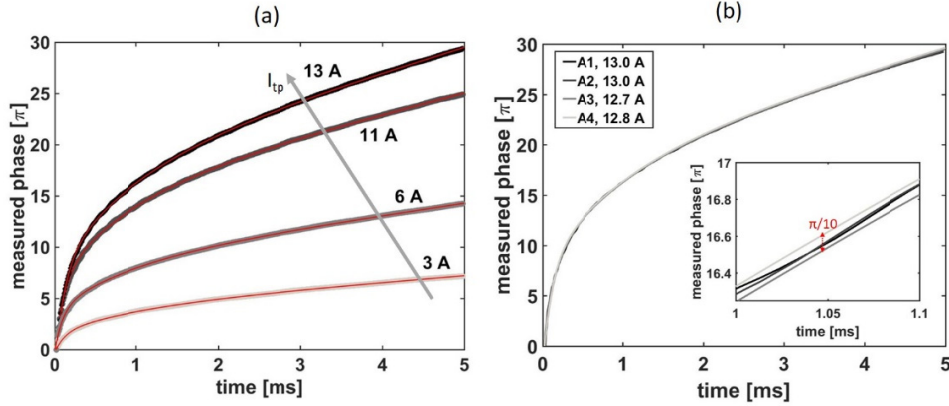


Fig. 3. (a) Measured piston phase drift during QCW operation of amplifier 1 at different currents into the tapered section. The experimental data is plotted as thick grayscale data points and the fitted function as a red solid line. (b) Measured phase drift during QCW operation for all four amplifiers. The currents into the taper were slightly adjusted around 13 A in order to achieve the same phase drift and balance slight differences in the efficiency of the devices. The inset shows a zoom into the same data in order to distinguish the different solid lines. (Bias conditions for all measurements: $P_{in} = 20$ mW, $I_{rw} = 350$ mA, $T = 25^\circ\text{C}$, $\Delta t_{QCW} = 5$ ms, 10 % duty cycle)

3.3 Power stability in QCW mode

We measured the pulse stability at different currents into the tapered section and observed oscillations in the output power as shown in Fig. 4. The period of the oscillations is increasing with time and decreasing with the current into the taper, although there were minor differences between the amplifiers used. The best ones (see amplifier 1, black lines) show significant but stable oscillations at very high currents only. The peak-to-peak amplitude of the oscillations measured at 16 A for amplifier 1 are below 6 % of the average power. Devices with a slightly lower performance (see amplifier 2 above) tended to show stronger oscillations at moderate currents (10-12 A) and the oscillations become chaotic at high currents (e.g. 16 A) with a peak-to-peak amplitude of about 12 %.

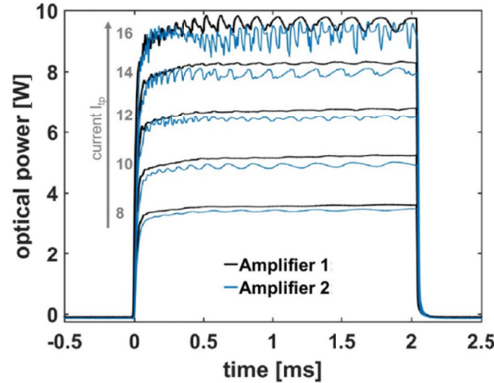


Fig. 4. Measured pulse shape for two amplifiers at 8-16 A current into the tapered section (Bias conditions for all measurements: $P_{in} = 20$ mW, $I_{rw} = 350$ mA, $T = 25^\circ\text{C}$, $\Delta t_{QCW} = 2$ ms, 10 % duty cycle).

These quasi-periodic oscillations are attributed to parasitic resonances of the narrow spectral line seed signal ($\Delta\nu_{FWHM} < 20$ MHz) within the amplifier. Indeed though both device facets are AR coated ($R_1 = 0.01$ % and $R_2 = 0.05$ %), the amplifier acts as a low-finesse

scanning Fabry-Perot cavity whose resonance peaks shift during the current pulse following the dynamic phase drift $\varphi(t)$ discussed earlier. Consequently, the period of the oscillations increases during the pulse (cf. Fig. 3 and Eq. 1). Furthermore the cavity finesse is enhanced with the amplifier gain, leading to an increase of the modulation depth. The slight disparities in the behavior of the different devices are therefore attributed to small differences in the coating reflectivity, coupling efficiency and gain in the device.

It would be desirable for further studies to use amplifiers with the best possible AR-coating on both facets in order to push the onset of these oscillations to even higher powers, which was not possible in the framework of this work. Besides the degradation of the beam quality at high bias, the poor pulse stability is another limitation for power scaling by QCW operation in QCW mode. Especially regarding coherent superposition, it is important to have a reasonable stability of the power within the pulse. We therefore limited the current in the tapered section to below 14.5 A for the subsequent CBC experiments, as the pulse stability was insufficient at higher currents.

3.4 Optical feedback from overdriven tapered amplifiers

It is well known that optical feedback from a distant reflector may perturb the lasing properties of a DFB laser, such as frequency, spectral linewidth and power [27]. In particular, weak time-dependent feedback may lead to a rich variety of effects including frequency hopping. We started our experiment with one double-stage Faraday isolator (-55 dB optical isolation) between the seed DFB laser diode and the CBC interferometer to limit reflection effects. A small part of the amplified beam gets reflected at the output facet ($R_2 = 0.5\%$) of the amplifier and propagates backwards through the setup towards the seed laser. This optical feedback is spectrally identical to the seed laser with only minor ASE contribution. As several parallel overdriven tapered amplifiers lead to high levels of absolute optical feedback, it appears that this isolation was not sufficient to prevent perturbations of the seed laser. Indeed we measured the seed laser frequency using a Fabry-Perot interferometer (Thorlabs SA210-8B, FSR = 10 GHz, finesse > 150). Figure 5(a) shows the measured seed laser frequency perturbations (blue line) induced by optical feedback from one tapered amplifier during a 5 ms-long QCW pulse (black line). The feedback leads to a frequency shift and a frequency hopping up to 80 MHz. The decreasing period of the observed frequency hopping appears to be linked to the phase dynamics discussed in section 3.2.

In the presence of an optical feedback, the frequency shift of a single-mode laser is described by [27]

$$\Delta \nu(t) = \nu(t) - \nu_0 = -\frac{\kappa}{2\pi} \left[\sin(2\pi \nu(t) \times \tau_e(t)) + \alpha \times \cos(2\pi \nu(t) \times \tau_e(t)) \right], \quad (2)$$

with the coupling coefficient

$$\kappa = \frac{(1 - R_s) \sqrt{R_e}}{\tau_s \sqrt{R_s}}, \quad (3)$$

where R_s is the reflectivity of the laser output facet, R_e is the effective reflectivity of the external optical setup, τ_s is the roundtrip time in the laser, $\tau_e(t)$ is the time dependent round trip time of the feedback and α is the linewidth enhancement factor. Frequency hopping occurs for higher levels of the product $\kappa \tau_e$ when there are multiple solutions for Eq. 2. We calculated the frequency change using the measurement of the phase drift at $I_{\text{tp}} = 13$ A given in Fig. 3(a) for defining $\tau_e(t)$ with $\tau_e(0) = 10$ ns related to the distance from the seed laser to the amplifier (about 1.5 m in this laboratory scale experiment). We compared in Figs. 5(a) and 5(b) the experimental evolution of the seed frequency during the pulse with a numerical resolution of Eq. 2. Each black dot in Fig. 5(b) is one calculated solution to this equation. We can easily identify regimes with multiple solutions where frequency hopping is likely to

occur. The red line represents the expected evolution of the seed laser frequency, assuming that the frequency hopping occurs when the change in the laser frequency has reached the local minimum. Fig. 5(a) shows that the measurement (blue) and simulation (red) are in good agreement during the whole pulse. The value for the external reflection of the extended cavity $R_e = 9 \times 10^{-10}$ used in these simulations may appear low but corresponds to the small part of the optical feedback from the amplifier that couples back into the seed laser. Indeed feedback from a distant reflector is critical even at very low level (see [27]). In comparison feedback from near passive optical elements (such as L_1 in Fig 1.) may have a similar level, but would be less critical as it would be induced at short distance and would result in a stable piston phase.

Equation (2) has multiple solutions, resulting in frequency hopping, if $\sqrt{1 + \alpha^2} \kappa \tau_e > 1$.

With our simulation parameters, the product $\sqrt{1 + \alpha^2} \kappa \tau_e$ was equal to about 2.44. As $\kappa \propto \sqrt{R_e}$ we estimate that the optical isolation in our experimental conditions should be better than -62.7 dB to avoid those frequency hops. Furthermore the maximum change in frequency would be below 10 MHz for an optical isolation better than -73 dB considering that $\Delta\nu \propto \sqrt{R_e}$. We repeated our experiment after increasing the optical isolation from -55 dB to -75 dB by using a third stage of optical isolation and did no longer measure any effect on the laser frequency during the QCW pulses. We conclude that the requirements regarding the optical isolation of a narrow linewidth seed laser can be extremely high in CBC architectures, especially when the amplifiers are overdriven and generate therefore a high level of feedback. The sensitivity to optical feedback could be reduced in an integrated optical setup (to minimize τ_e), by increasing the reflectivity R_s of the seed laser and by further improvement of the AR coatings of the tapered amplifiers (to reduce R_e). Small perturbations of the seed laser frequency in the range of 80 MHz (see Fig. 5(a)) are not necessarily a problem for successful CBC, as this corresponds still to a coherence length in the range of 1 m, but is critical for applications requiring a stable frequency.

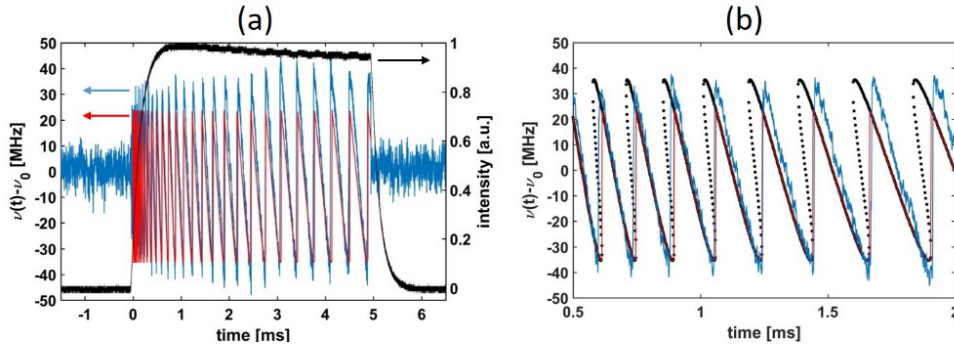


Fig. 5. (a) Measurement of the seed laser frequency perturbations $\nu(t) - \nu_0$ (blue), and simulated laser frequency perturbations (red) induced by optical feedback from a single tapered amplifier (A1) operated at $I_p = 13$ A (black). (b) Zoom into the measured frequency change with the calculated solutions (black dots) for the seed laser frequency considering the phase change in the amplifier and the expected frequency hopping in the multi-stable regime (red solid line). The simulation parameters used were: $\alpha = 5$, $R_s = 0.01$, $R_e = 9 \times 10^{-10}$, $\tau_s = 50$ ps, $\tau_e(t) = 10$ ns + $\frac{\lambda \varphi(t)_{13A}}{\pi c}$, where $\varphi(t)_{13A}$ was taken from Fig 3(a)). The optical isolation was -55 dB.

4. Coherent beam combining in QCW operation

The phase matching between the four amplified beams in the coherent beam combining experiment was achieved by a sequential hill-climbing algorithm with stepwise adjustment of the current into the RW from pulse to pulse. The error signal was measured with a fast

photodiode (see Fig. 1) measuring the power at the CBC output. The currents into the amplifiers were optimized separately: the current into the RW of A2 was optimized first from pulse to pulse, then the current into A3 similarly and finally the current into A4. A variation of ± 35 mA corresponded to a phase shift of $\pm\pi$ and we used steps of 0.75 mA for the hill-climbing algorithm. Phase control with this simple sequential pulse-to-pulse algorithm was sufficient as the phase noise in the interferometer was dominated by very low frequencies (<1 Hz). The feedback loop was triggered to maximize the power of the combined beam after 50 % of the pulse duration as the pulse stability was better in the second half of the pulse (cf. Fig. 4). The pulse duration was adjustable from 1 to 10 ms and the duty cycle from 0.01 to 10 % (we typically used 2 ms pulses and a duty cycle of 10 %). The achieved coherently combined power P_{CBC} and the corresponding combining efficiency, defined as the ratio of the combined power over the sum of the individual powers ($\eta_{CBC} = P_{CBC} / \sum_1^4 P_i$), are summarized in Table 1. Power and combining efficiency for operation in continuous wave mode are also given for comparison. The current values I_{ip} into the tapered section correspond to the average of the four currents, which were slightly adjusted in order to optimize the phase matching during the pulse (see Fig. 3 (b)). For each measurement, the SA cylindrical lenses (L_4 see Fig. 1) were positioned to compensate for the amplifier astigmatism and optimize the overlap of the beams during the current pulse despite the wandering SA waist position mentioned in section 3.1.

At the maximum operating current $I_{ip} = 14.5$ A per amplifier the QCW output power of the coherently combined output beam reached 22.7 W. This is the highest power reported for CBC of tapered lasers or amplifiers. In contrast we measured 16.9 W as the highest power in CW, which is about 25 % lower than the maximum QCW power. The combining efficiency at the highest bias was $> 64\%$ limited by the degradation of the beam quality at high currents. The combining efficiency at moderate currents was measured to be $> 70\%$ and almost identical for QCW and CW operation. The combining efficiency of the coherent superposition of only two amplifiers was slightly higher, in the range of 79-84 %, as each combining step adds combining losses.

Table 1. Measured combined power P_{CBC} and combining efficiency for coherent superposition of two (A1+A2) and four (A1+A2+A3+A4) amplifiers at different currents into the tapered sections. Operating conditions for each individual amplifier: $P_{in} = 20$ mW, $I_{rw} = 300$ -400 mA, $T = 25^\circ\text{C}$, $\Delta t_{qcw} = 2$ ms, 10 % duty cycle.

I_{ip} [A]	QCW				CW	
	2 amplifiers		4 amplifiers		4 amplifiers	
	P_{CBC} [W]	η_{CBC} [%]	P_{CBC} [W]	η_{CBC} [%]	P_{CBC} [W]	η_{CBC} [%]
8	-	-	-	-	10.8	72
10	9.77	84	16.8	71	14.4	71
12.3	12.4	85	20.4	68	16.9	71
13	12.7	81	21.7	69	-	-
14.5	13.7	79	22.7	64	-	-

A large part of the combining losses were attributed to a spatial clean-up of the beam. The beam from each amplifier has a central lobe power content in the order of 75 % (cf. Fig. 2), which is significantly lower than the central lobe power content of the coherently combined beam of 92 % as shown in Fig. 6. The M^2 beam propagation factor of the combined beam was below 1.3 in both directions considering the $1/e^2$ beam diameters. The more accurate and standard definition of the M^2 factor, using the 2nd moment beam diameters, resulted in 1.3 in FA and 5 in SA : this is below the beam propagation factor of the individual amplifiers $M^2 >$

10 in SA at high bias. The improved beam quality of the combined beam (evidenced by higher central lobe power content and improved M^2) is typical for coherent beam combining of tapered lasers and amplifiers [12,13]. It is related to a high mismatch in amplitude and phase of the higher order modal content in the individual beams, whereas the central lobes of those individual beams have a high spatial overlap and interfere efficiently. The combining efficiency considering the central lobe powers only was $>80\%$ for the whole setup. Slight mismatches in the FA collimation and the parasitic resonances (cf. section 3.3 and Fig. 4) were identified as the limitation for further increase in combining efficiency.

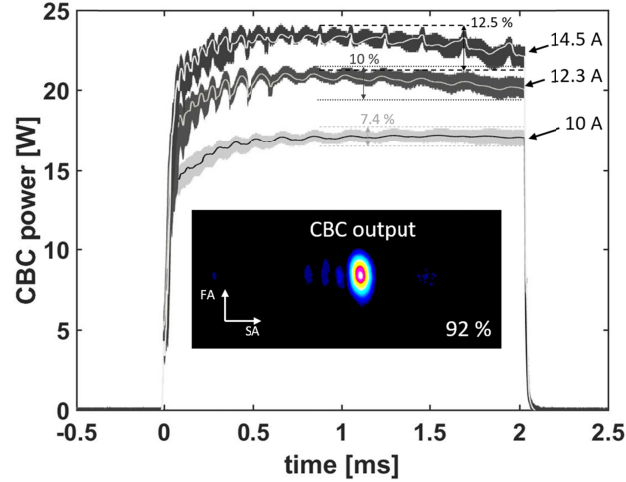


Fig. 6. Measured pulse shape at the output of the CBC interferometer at 10 A, 12.3 A and 14.5 A into each tapered section. At each bias we measured the envelope (1 min integration time) (see thick lines) and the average pulse shape (thin line). The inset shows the waist of the combined beam at the highest bias current and the measured power content in the central lobe. (Bias conditions for all measurements: $P_{in} = 20$ mW, $I_{rw} = 300-400$ mA, $T = 25^\circ\text{C}$, $\Delta t_{qew} = 2$ ms, 10 % duty cycle).

Figure 6 shows the measured pulse stability at three different bias points. We measured the envelope of the pulses over one minute (see thick lines) and the average pulse shapes (see thin lines). The peak to valley roughness of the pulse envelope increases from 7.4 % at 10 A to 12.5 % at 14.5 A, mainly caused by the resonance effects in the amplifiers analyzed in section 3.3, with (feedback-induced) instability in the seed source eliminated by using high levels of optical isolation (-75 dB). CBC at even higher bias was unstable as the internal resonance effects perturb the phase control and the oscillations get chaotic. The beam quality of the combined beam was close to the diffraction limit and improved compared to the beam quality of an individual amplifier. This beam clean-up is a typical effect of CBC with tapered lasers or amplifiers [9,13]. The power content in the central lobe of the output beam was $> 92\%$, with only a few higher angle side lobes in SA. The evaluated central lobe power was > 20 W at 14.5 W, which is the highest diffraction limited power reported for a single coherent beam from tapered lasers or amplifiers and is an extremely high value for a single frequency semiconductor based system.

5. Conclusion

In this paper we investigated the dynamics of high power tapered amplifiers in pulsed quasi-continuous operation. The rise in temperature as the device is turned on leads to a change in the beam shape in SA caused by a wandering astigmatism. The phase drift is also related to the rising temperature in the device and was measured for different bias currents in the tapered section. It was shown that good phase matching with residual errors below $\pi/10$ can

be achieved even at high currents. Power instabilities in the QCW pulses occur at high bias as resonances in the device interfere with the seed laser beam. Further increase of the current into the taper was limited by the pulse stability and the decreasing beam quality.

CBC of four tapered amplifiers in QCW lead to a total power of 22.7 W with 64 % combining efficiency. The advantage in using tapered amplifiers for CBC is the extremely high power per device (here 5.67 W per amplifier) that exceeds the power achievable with single-mode amplifiers by more than a factor of 5. Higher total powers have so far only been achieved by coherent beam combining of large arrays of single-mode amplifiers at the cost of an increased complexity (CBC of 47 single-mode slab-coupled optical waveguide amplifiers yielded 40 W [11]). The achieved power in the central lobe of the combined beam is higher than 20 W (92 % of total power). This is the highest power in a diffraction-limited beam ever reported from a single-frequency system based on tapered lasers or amplifiers. The operation in QCW mode allowed to overcome thermal limitations and to reach about 25 % higher power in comparison to CW operation.

The power could be further increased by using more efficient semiconductor structures, either directly as here or fabricated as single-contact truncated tapered amplifiers, which provide the highest reported diffraction limited power (QCW power in the central lobe up to 17 W per device [22]). Higher powers are also likely to be possible by using lower reflectivity coatings and tilted facets on the tapered amplifiers to suppress internal oscillations. Combining these approaches offers a potential path for the development of compact CBC modules exceeding 50 W output power with close to diffraction limited beam quality. Efforts to reduce the pulse durations to the microsecond and nanosecond regime are also promising for potential applications in biomedicine [15,16] and remote sensing [18,19].

Acknowledgments

The authors are grateful to all colleagues involved into device fabrication and mounting at the Ferdinand-Braun-Institut in Berlin.

Parts of this work have been previously been presented at the CLEO®/Europe-EQEC 2019 conference in Munich, Germany (Paper CB-4.6).

References

1. F. Bachmann, P. Loosen, and R. Poprawe, eds., *High Power Diode Lasers: Technology and Applications*, Springer Series in Optical Sciences (Springer-Verlag, 2007).
2. T. Y. Fan, "Laser beam combining for high-power, high-radiance sources," *IEEE J. Sel. Top. Quantum Electron.* **11**, 567–577 (2005).
3. S. Strohmaier, C. Tillkorn, P. Olschowsky, and J. Hostetler, "High-power, high-brightness direct-diode lasers," *Optics and Photonics News* **21**, 24–29 (2010).
4. V. Daneu, A. Sanchez, T. Y. Fan, H. K. Choi, G. W. Turner, and C. C. Cook, "Spectral beam combining of a broad-stripe diode laser array in an external cavity," *Opt. Lett.* **25**, 405–407 (2000).
5. L. Bartelt-Berger, U. Brauch, A. Giesen, H. Huegel, and H. Opower, "Power-scalable system of phase-locked single-mode diode lasers," *Appl. Opt.* **38**, 5752–5760 (1999).
6. B. Liu, Y. Liu, and Y. Braiman, "Coherent addition of high power laser diode array with a V-shape external Talbot cavity," *Opt. Expr.* **16**, 20935–20942 (2008).
7. D. Paboef, G. Lucas-Leclin, P. Georges, N. Michel, M. Krakowski, J. Lim, S. Sujecki, and E. Larkins, "Narrow-line coherently combined tapered laser diodes in a Talbot external cavity with a volume Bragg grating," *Appl. Phys. Lett.* **93**, 211102 (2008).
8. J. Montoya, S. J. Augst, K. Creedon, J. Kinsky, T. Y. Fan, and A. Sanchez-Rubio, "External cavity beam combining of 21 semiconductor lasers using SPGD," *Appl. Opt.* **51**, 1724–1728 (2012).
9. G. Schimmel, I. Doyen-Moldovan, S. Janicot, M. Hanna, J. Decker, P. Crump, G. Blume, G. Erbert, P. Georges, and G. Lucas-Leclin, "Rear-side resonator architecture for the passive coherent combining of high-brightness laser diodes," *Opt. Lett.* **41**, 950–953 (2016).
10. S. M. Redmond, K. J. Creedon, J. E. Kinsky, S. J. Augst, L. J. Missaggia, M. K. Connors, R. K. Huang, B. Chann, T. Y. Fan, and G. W. Turner, "Active coherent beam combining of diode lasers," *Opt. Lett.* **36**, 999–1001 (2011).
11. K. J. Creedon, S. M. Redmond, G. M. Smith, L. J. Missaggia, M. K. Connors, J. E. Kinsky, T. Y. Fan, G. W. Turner, and A. Sanchez-Rubio, "High efficiency coherent beam combining of semiconductor optical amplifiers," *Opt. Lett.* **37**, 5006–5008 (2012).

12. G. Schimmel, S. Janicot, M. Hanna, J. Decker, P. Crump, G. Erbert, U. Witte, M. Traub, P. Georges, and G. Lucas-Leclin, "Coherent beam combining architectures for high power tapered laser arrays," in Proc. SPIE 10086, 100860O (2017).
13. P. Albrodt, M. T. Jamal, A. K. Hansen, O. B. Jensen, G. Blume, K. Paschke, P. Crump, P. Georges, and G. Lucas-Leclin, "Coherent combining of high brightness tapered amplifiers for efficient non-linear conversion," Opt. Exp. **27**, 928–937 (2019).
14. J. S. Osinski, D. Mehuys, D. F. Welch, R. G. Waarts, J. S. Major, K. M. Dzurko, and R. J. Lang, "Phased array of high power, coherent, monolithic flared amplifier master oscillator power amplifiers," Appl. Phys. Lett. **66**, 556–558 (1995).
15. B. Gupta, M. Elagouz, D. McHugh, V. Chong, and S. Sivaprasad, "Micropulse diode laser photocoagulation for central serous chorio-retinopathy," Clinical & Experimental Ophthalmology **37**, 801–805 (2009).
15. L. Chehade, G. Chidlow, J. Wood, and R. J. Casson, "Short-pulse duration retinal lasers: a review," Clinical & Experimental Ophthalmology **44**, 714–721 (2016).
17. M. Christensen, A. K. Hansen, D. Noordegraaf, O. B. Jensen, and P. M. W. Skovgaard, "Deep modulation of second-harmonic light by wavelength detuning of a laser diode," Appl. Opt. **56**, 2250–2254 (2017).
18. A. R. Nehrir, K. S. Repasky, and J. L. Carlsten, "Eye-Safe Diode-Laser-Based Micropulse Differential Absorption Lidar (DIAL) for Water Vapor Profiling in the Lower Troposphere," Journal of Atmospheric and Oceanic Technology **28**, 131–147 (2011).
19. A. R. Nehrir, K. S. Repasky, and J. L. Carlsten, "Micropulse water vapor differential absorption lidar: transmitter design and performance," Opt. Expr. **20**, 25137–25151 (2012).
20. R_2 was slightly higher as these amplifiers have been designed for backside extended cavity configurations in the first place, where a weak feedback from R_2 was necessary.
21. P. Crump, J. Decker, M. Winterfeldt, J. Fricke, A. Maaßdorf, G. Erbert, and G. Tränkle, "Development of high-power diode lasers with beam parameter product below 2 mm mrad within the BRIDLE project," in Proc SPIE 9348, 93480D (2015).
22. X. Wang, G. Erbert, H. Wenzel, P. Crump, B. Eppich, S. Knigge, P. Ressel, A. Ginolas, A. Maassdorf, and G. Tränkle, "17-W Near-Diffraction-Limited 970-nm Output From a Tapered Semiconductor Optical Amplifier," IEEE Phot. Techn. Lett. **25**, 115–118 (2013).
23. P. Albrodt, M. Hanna, F. Moron, J. Decker, M. Winterfeldt, G. Blume, G. Erbert, P. Crump, P. Georges, and G. Lucas-Leclin, "Coherent combining of high brightness tapered lasers in master oscillator power amplifier configuration," in Proc. SPIE 10514, 105140T (2018).
24. L. Borruel, S. Sujecki, P. Moreno, J. Wykes, M. Krakowski, B. Sumpf, P. Sewell, S.-C. Auzanneau, H. Wenzel, D. Rodriguez, T. M. Benson, E. C. Larkins, and I. Esquivias, "Quasi-3-D simulation of high-brightness tapered lasers," IEEE J. Quantum Electron. **40**, 463–472 (2004).
25. M. T. Kelemen, J. Weber, S. Kallenbach, C. Pfahler, M. Mikulla, and G. Weimann, "Astigmatism and beam quality of high-brightness tapered diode lasers," in Proc. SPIE **5452**, 233 (2004).
26. P. Albrodt, M. T. Jamal, A. K. Hansen, O. B. Jensen, M. Niemeyer, G. Blume, K. Paschke, P. Crump, J. Hamperl, P. Georges, and G. Lucas-Leclin, "Recent progress in brightness scaling by coherent beam combining of tapered amplifiers for efficient high power frequency doubling," in Proc. SPIE 10900, 109000O (2019).
27. R. Tkach and A. Chraplyvy, "Regimes of feedback effects in 1.5- μ m distributed feedback lasers," J. Lightwave Technol. **4**, 1655–1661 (1986).